Functional & Integrative Genomics (2025) 25:59
https://doi.org/10.1007/s10142-025-01574-5

RESEARCH

MAZ-mediated LAMA5 transcription activation promotes gastric cancer progression through the STAT3 signaling

Yu Wang[1] · Jiazhong Xu[1] · Hongxia Zhang[2] · Xiaobo Guo[1] · Hongjun Liu[1] · Qinhui Sun[1]

Received: 12 November 2024 / Revised: 26 February 2025 / Accepted: 5 March 2025

Abstract

Laminin subunit alpha-5 (LAMA5) has been identified as an oncogene in many cancers, while its role and mechanism in gastric cancer (GC) remain to be explored. Here, the influences of LAMA5 knockdown on GC were investigated in vitro and in vivo. LAMA5 expression was silenced in GC cells alone or in combination with the signal transducer and activator of transcription 3 (STAT3) activator Colivelin, followed by CCK-8, colony formation, EdU, flow cytometry, wound healing assay, and Transwell assay. The regulatory relationship between Myc-associated zinc finger protein (MAZ) and LAMA5 was characterized by ChIP and luciferase reporter analysis. The effect of knockdown of MAZ alone or in combination with LAMA5 overexpression on GC was investigated in vitro and in vivo. LAMA5 was highly expressed in GC cells, and knockdown of LAMA5 inhibited GC cell malignant aggressiveness, which was reversed by the Colivelin treatment. The transcription factor MAZ bound to the promoter of LAMA5 to activate its transcription, and the anti-tumor effects of sh-MAZ on GC cells in vitro and in vivo were overturned by LAMA5 overexpression. In conclusion, MAZ promotes GC cell proliferation and migration by the LAMA5/STAT3 axis, implying that this axis can function as a target for GC therapy.

Keywords Gastric cancer · LAMA5 · STAT3 · MAZ · Colivelin

Introduction

Gastric cancer (GC) ranks fourth in terms of cancer-related mortality and stands as the fifth most prevalent cancer in the world range (Christodoulidis et al. 2024). Even though systemic therapies for GC, including chemotherapy, targeted therapy, and immunotherapy, have evolved significantly, these patients still have a poor prognosis (Alsina et al. 2023; Guan et al. 2023). Moreover, the global burden of this malignancy is expected to have a 62% increase by 2040 (Thrift et al. 2023). Therefore, there is an urgent need to understand the mechanisms underlying GC development further and develop more effective strategies to counteract GC progression.

The laminin family represents one of the most widely expressed extracellular matrix proteins and exerts many important functions in multiple organs/systems (Yao 2017). For instance, the laminin subunit gamma-2 (LAMC2) expression was markedly upregulated in GC cell lines, and LAMC2 silencing substantially repressed GC cell growth, migration, and invasion (Cheng et al. 2024). In the present study, we identified laminin subunit alpha-5 (LAMA5) as a differentially expressed gene in GC tissues relative to adjacent tissues with outstanding prognostic value in the GEO datasets. LAMA5 has been reported to promote cell proliferation and migration in ovarian cancer (Diao et al. 2023). However, its functional role and the molecular mechanism involved in GC has not been revealed. Interestingly, the LAMA5/signal transducer and activator of transcription 3 (STAT3) axis have been implicated in the acinar-to-ductal cell transdifferentiation induced by cancer-associated fibroblast in pancreatic ductal adenocarcinoma (Parte et al. 2024), and the oncogenic role of STAT3 in GC has been verified in our previous study (Cui et al. 2021). We hypothesize

✉ Qinhui Sun
sunqh0115@126.com

[1] Department of Gastrointestinal Surgery, Shandong Provincial Hospital Affiliated to Shandong First Medical University, No. 324, Jingwu Road, Huaiyin District, Jinan, Shandong 250021, P.R. China

[2] Department of Laser Cosmetic Clinic, Shandong Provincial Hospital Affiliated to Shandong First Medical University, Jinan, Shandong 250021, P.R. China

Published online: 12 March 2025

that LAMA5 expedites GC growth by inducing the STAT3 pathway. Myc-associated zinc finger protein (MAZ) is a transcription factor with C2H2-type zinc-finger motifs that activates the transcription of some cancer-related genes and represses that of others, thereby playing different roles in the progression of different types of cancers depending on its targets (Yu et al. 2017). Under the condition of thyroid cancer, patients with high MAZ expression had shorter overall and disease-free survival compared with patients with low MAZ expression (Zheng et al. 2023). In addition, silencing of MAZ repressed the invasion and migration abilities of prostate cancer cells in vitro and bone metastasis ability in vivo through transcriptionally upregulating KRas and HRas expression (Yang et al. 2019). However, the effects of MAZ on the LAMA5/STAT3 axis in GC remain unexplored, and this area deserves further investigation.

Materials and methods

Cell culture, treatment, and lentiviral production and infection

The human gastric epithelial cells GES1 were purchased from BeNa Culture Collection (Beijing, China), and the human GC cell lines AGS and HGC27 were purchased from Procell (Wuhan, Hubei, China). All cell lines were cultured in Dulbecco's modified Eagle's medium (DMEM, 30030, Gibco, Carlsbad, CA, USA) containing 10% fetal bovine serum (E510008, Shanghai Sangon Biological Engineering Technology & Services Co., Ltd., Shanghai, China) with 5% CO_2 at a temperature of 37℃.

GC cells were infected with sh-NC, sh-LAMA5, sh-MAZ, sh-MAZ+oe-NC, and sh-MAZ+oe-LAMA5 lentiviral vectors, which were all purchased from VectorBuilder (Guangzhou, Guangdong, China), at a titer of 10^8 TU/mL, followed by treatment with puromycin (5 μg/mL, ST551, Beyotime Biotechnology Co., Ltd., Shanghai, China) for 10 days to obtain stable cells. AGS and HGC27 cells infected with sh-LAMA5 were pretreated with 0.5 μM STAT3 activator Colivelin (HY-P1061, MedChemExpress, Monmouth Junction, NJ, USA) (Chiu et al. 2016) or DMSO for 1 h for subsequent experiments.

Cell proliferation assay

GC cells were plated in 96-well plates with a cell density of 3.0×10^3 cells/well. After incubation for 24 h, 48 h, and 72 h, each well was placed in 10 μL of cell counting kit-8 (CCK8) reagent (E606335, Sangon) and incubated at 37 °C for 2 h. The optical density (OD) value at 450 nm was measured using a microplate reader.

Colony formation assay

Infected cells were placed in each well of a 6-well plate at a cell density of 500 cells/well and maintained in a medium containing 10% FBS for 2 weeks, during which time the medium was changed every 4 days. Colonies were fixed using paraformaldehyde and stained with 0.1% crystal violet (C0775, Sigma-Aldrich Chemical Company, St Louis, MO, USA) in PBS for 15 min. Colony formation was determined by counting the number of stained colonies.

Cell viability assay

EdU staining experiments were performed according to the instructions of the BeyoClick EdU-594 Cell Proliferation Assay Kit (C0078L, Beyotime). Briefly, the cells were cultured in 6-well plates and incubated with 20 μM EdU working solution pre-warmed at 37 °C for 2 h. After EdU labeling of cells was completed, the cells were fixed with 1 mL of 4% paraformaldehyde for 15 min, incubated with 1 mL of PBS containing 0.3% Triton X-100 for 10 min, and with 0.5 mLClick reaction solution for 30 min in the dark, and counter-stained for 10 min in the dark (all at room temperature). Images were taken using fluorescence microscopy, and the EdU-positive cell rate was calculated.

Wound healing assay

The GC cells were grown in 6-well plates and incubated with DMEM containing 10% FBS until 90% confluence was reached. After that, the cells were incubated with serum-free DMEM. Several vertical lines were scratched on the cell surface using a 10 μL pipette tip, and non-adherent cells were removed by washing the plate using PBS. Photographs of migrated cells were taken after 0 h and 24 h of incubation to detect the wound closure rate.

Transwell assays

Migration assays and invasion assays were performed using 24-well Transwell chambers (CLS3378, Sigma-Aldrich). The apical chamber was pre-coated with Matrix-Gel (C0372, Beyotime) diluted at 1:8, no pre-coating was required for the migration test. According to the manufacturer's instructions, 1.0×10^5 live cells were seeded in the apical chamber and incubated with serum-free DMEM, while 700 μL of DMEM containing 10% FBS was added to the basolateral chamber. After 48 h of incubation, the cells and Matrix-Gel were carefully removed from the membrane in the apical chamber with a cotton swab. Migrated or invaded cells on the bottom surface of the membrane were fixed with 4%

paraformaldehyde and stained with 0.5% crystal violet. Finally, stained cells in five random fields were counted and photographed under an inverted microscope for quantitative analysis.

Cell apoptosis by flow cytometry

Apoptosis was assessed using Annexin V-FITC/PI double staining apoptosis detection kit (G003-1-2, Nanjing JianCheng Bioengineering Institute, Nanjing, Jiangsu, China). Sample cells were seeded and incubated in 6-well plates, detached with trypsin, and resuspended in a binding buffer. The cells were incubated with 5 μL of Annexin V-FITC and 5 μL of PI for 15 min, and apoptosis was detected using flow cytometry.

Mouse xenografts

Animal experiments were approved by the Animal Care and Ethics Committee of Shandong Provincial Hospital Affiliated to Shandong First Medical University (approval no. KT2024-01-15-01). Six-week-old female BALB/c mice (18 ± 2 g) were procured from Vital River (Beijing, China). AGS and HGC27 (1.0×10^7 cells/200 μL) cells infected with sh-NC or sh-MAZ and AGC cells infected with sh-MAZ + oe-NC or sh-MAZ + oe-LAMA5 were mixed with Geltrex Matrigel in a 1:1 ratio, respectively and injected into the dorsal side of female BALB/c mice using subcutaneous injection. Tumor volume (V) was calculated by the following formula: $V = \text{length} \times \text{width}^2/2$ every four days. Mice were humanely euthanized on d 16 by intraperitoneal injection of 150 mg/kg sodium pentobarbital, and xenograft tumors were obtained and weighed.

RNA isolation, reverse transcription (RT) and quantitative polymerase chain reaction (RT-qPCR)

Total RNA was extracted from GC cells or mouse tumor tissues using TRIzol reagent (12183555, Gibco), and the purity and concentration of RNA were measured by spectrophotometry. Reverse transcription of mRNA was performed using the RT Kit (RT31-020, QIAGEN GmbH, Hilden, Germany) according to the manufacturer's instructions. This was followed by quantification using BeyoFast SYBR Green qPCR Mix (D7260, Beyotime) on a CFX Connect Real-Time System with a real-time PCR system. Glyceraldehyde-3-phosphate dehydrogenase (GAPDH) was considered as an internal control. The $2^{-\Delta\Delta Ct}$ method was used to calculate relative mRNA expression. The primers (all obtained from OriGene Technologies, Beijing, China) are as follows: LAMA5 forward, 5′-AACCAGATGAGCATCA CATTCCTG-3′ and reverse, 5′-ACAGTGTTGCGCGTCT CCGTAT-3′; MAZ forward, 5′-GGATCACCTCAACAGT CACGTC-3′ and reverse, 5′-GGCACTTTCTCCTCGTGT CGTA-3′; GAPDH forward, 5′- GTCTCCTCTGACTTCA ACAGCG-3′ and reverse, 5′- ACCACCCTGTTGCTGTAG CCAA-3′.

Western blot

Total proteins in GC cells were washed twice with cold PBS and lysed in RIPA buffer (P0013K, Beyotime) containing a mixture of proteinase inhibitors. After protein extraction, protein concentrations were quantified using the BCA Protein Assay Kit (ab102536, Abcam, Cambridge, UK). The protein samples were separated with 10% sodium dodecyl sulfate-polyacrylamide gel electrophoresis and transferred to a polyvinylidene difluoride membrane (ab133411, Abcam). After being sealed with 5% skimmed milk in tris-buffered saline containing 0.1% Tween-20 (TBST) for 2 h, the membranes were incubated with diluted primary antibodies at 4 °C overnight. The following primary antibodies used were LAMA5 (1/1000, ab184330, Abcam), STAT3 (1/1000, ab109085, Abcam), phospho-STAT3 (1/1000, ab76315, Abcam), Bcl-xl (1/1000, 2764, Cell Signaling Technologies, Beverly, MA, USA), c-Myc (1/2500, 700648, Thermo Fisher Scientific Inc., Waltham, MA, USA), MAZ (1/1000, PA5-106686, Thermo Fisher Scientific), GAPDH (1/1000, PA1-987, Thermo Fisher Scientific). On the second day, the PVDF membranes were rinsed five times with TBST solution (10 min each time), and incubated with diluted HRP-conjugated secondary antibody goat anti-rabbit IgG H&L (HRP) (1/2000, ab6721, Abcam) for 1 h at room temperature. Finally, the membranes were developed using ECL chemiluminescence.

Immunohistochemistry

Tumor tissues were harvested and fixed in 4% paraformaldehyde overnight, paraffin-embedded, and cut into 3-μm thick sections. Tissue sections were deparaffinized and rehydrated, followed by antigen retrieval in EDTA buffer at pH 9.0 and 1-h sealing using PBS containing 5% goat serum. Endogenous peroxidase activity was sealed by treating the sections with 3% hydrogen peroxide. The sections were incubated with the primary antibody against Ki-67 (1/1000, PA5-19462, Thermo Fisher) overnight at 4 °C and with secondary antibody goat anti-rabbit IgG H&L (HRP) (1/1000, ab6721, Abcam) at 37 °C for 50 min. DAB substrate was added to develop the color; hematoxylin was used to counter-stain the nuclei. Finally, microscopy was used for

imaging and analysis, and the results of the staining were characterized by the percentage of positive cell staining.

TUNEL

The apoptosis rate of xenograft tumors was determined using the One Step TUNEL Apoptosis Detection Kit (HY-K1078, MedChemExpress). Briefly, the paraffin-embedded sections were deparaffinized and incubated with proteinase K solution for 15 min at room temperature. Next, the TdT Enzyme was dissolved in FITC-12-dUTP Labeling Mix to configure the TUNEL working solution, and the sections were incubated with 50 μL of TUNEL working solution at 37 °C for 60 min in the dark, and the nuclei were stained with DAPI. After being sealed with an antifade mounting medium (HY-K1042, MedChemExpress), the fluorescence effect was observed under a fluorescence microscope.

Chromatin Immunoprecipitation (ChIP) assay

ChIP assay was performed using the ChIP Assay Kit (26157, Thermo Fisher) according to the manufacturer's instructions. AGS and HGC27 cells were added with formaldehyde for cross-linking. After the reaction was terminated by the glycine solution, the cell lysates were sonicated, and chromatin fragments were obtained by the addition of an MNase digestion buffer. Immunoprecipitation was performed overnight using the primary antibody to MAZ (NB100-86984, Novus Biological Inc., Littleton, CO, USA) or IgG antibody (ab172730, Abcam). A/G magnetic beads were added to adsorb chromatin fragments, followed by rinsing of the magnetic beads with IP elution buffer and sodium chloride solution. Finally, PCR amplification was performed using primers (LEFT PRIMER: 5'-AGCCGCTTCGCC ATCTTC-3'; RIGHT PRIMER: 5'-CCCCTCCTCTCTC CTTCCCC-3') specific for the LAMA5 promoter (chr20: 62367181–62367521).

Dual-luciferase reporter gene assay

The full-length fragment of the LAMA5 promoter (chr20: 62367181–62367521) was first obtained from UCSC (https://genome.ucsc.edu/index.html) to design the corresponding PCR primers. Sequences of amplified LAMA5 promoter fragments or LAMA5 promoter mutants (LAMA5 pro-Mut, chr20:62367260–62367270, chr20:62367356–623673366, chr20:62367418–623673428) were digested by KpnI and XhoI and ligated to pGL3 basic luciferase vector (212936, Addgene, Watertown, MA, USA) to construct the target plasmid. The constructed target plasmids were subsequently co-transfected with pRL Renilla Luciferase Control Reporter Vectors (E2241, Promega Corporation, Madison, WI, USA) into sh-NC and sh-MAZ treated GC cells. After 48 h, the cells were lysed. The supernatant was collected by centrifugation at 12,000 rpm for 1 min. The luciferase activity was assessed using the kit (16185, Thermo Fisher Scientific). The firefly luciferase activity was normalized to that of Renilla luciferase.

Statistics analyses

Results were presented as standard error of the mean (SEM). All statistical data were analyzed using GraphPad Prism software version 8.0 (GraphPad, San Diego, CA, USA). Statistical analysis between any two groups was performed using an unpaired t-test. One-way/two-way ANOVA, combined with Tukey's multiple-comparison test, was used to evaluate the statistical significance of differences among three or more groups. The significant difference is $p < 0.05$.

Results

Overexpression of LAMA5 in GC is predicted to be related to the dismal prognosis of patients

Three GC-related datasets GSE118916, GSE174237, and GSE224056 were included to analyze the differentially expressed genes with p adj < 0.05 as the screening threshold (adjusted by Benjamini & Hochberg). The volcano maps of GSE118916 (15 pairs of GC tumor and adjacent non-tumor tissues), GSE174237 (6 pairs of GC and paracancerous normal tissues), and GSE224056 (5 pairs of GC and adjacent tissues) are shown in Fig. 1A-C. The intersections of the differentially expressed genes screened from these three datasets were obtained from the Jvenn (https://jvenn.toulouse.inrae.fr/app/example.html) website ($n = 308$) (Fig. 1D). KEGG analysis was then performed at the KOBAS (http://bioinfo.org/kobas) website to rank the pathways in terms of p-value (Fig. 1E). Among the top three pathways (Human papillomavirus infection, Protein digestion and absorption, and Focal adhesion, ranked by p value), the focal adhesion pathway was noted since targeting focal adhesion proteins have been shown to sensitize tumor cells to different treatments, including radiotherapy, chemotherapy, and novel molecular therapeutics (Eke and Cordes 2015). For differentially expressed genes enriched to this pathway, the involvement of the collagen family (Romer et al. 2021), PDGF family (Tahara 1990), the THBS family (Lu et al. 2021), PRKCG (Li et al. 2022), and VAV2 (Sun et al. 2023) have been described in GC. In the GSE118916 database (LogFC = 1.362), GSE174237 (LogFC = 2.238), and GSE224056 database (LogFC = 1.176), LAMA5 was all highly expressed in GC tissues. Survival analysis in the

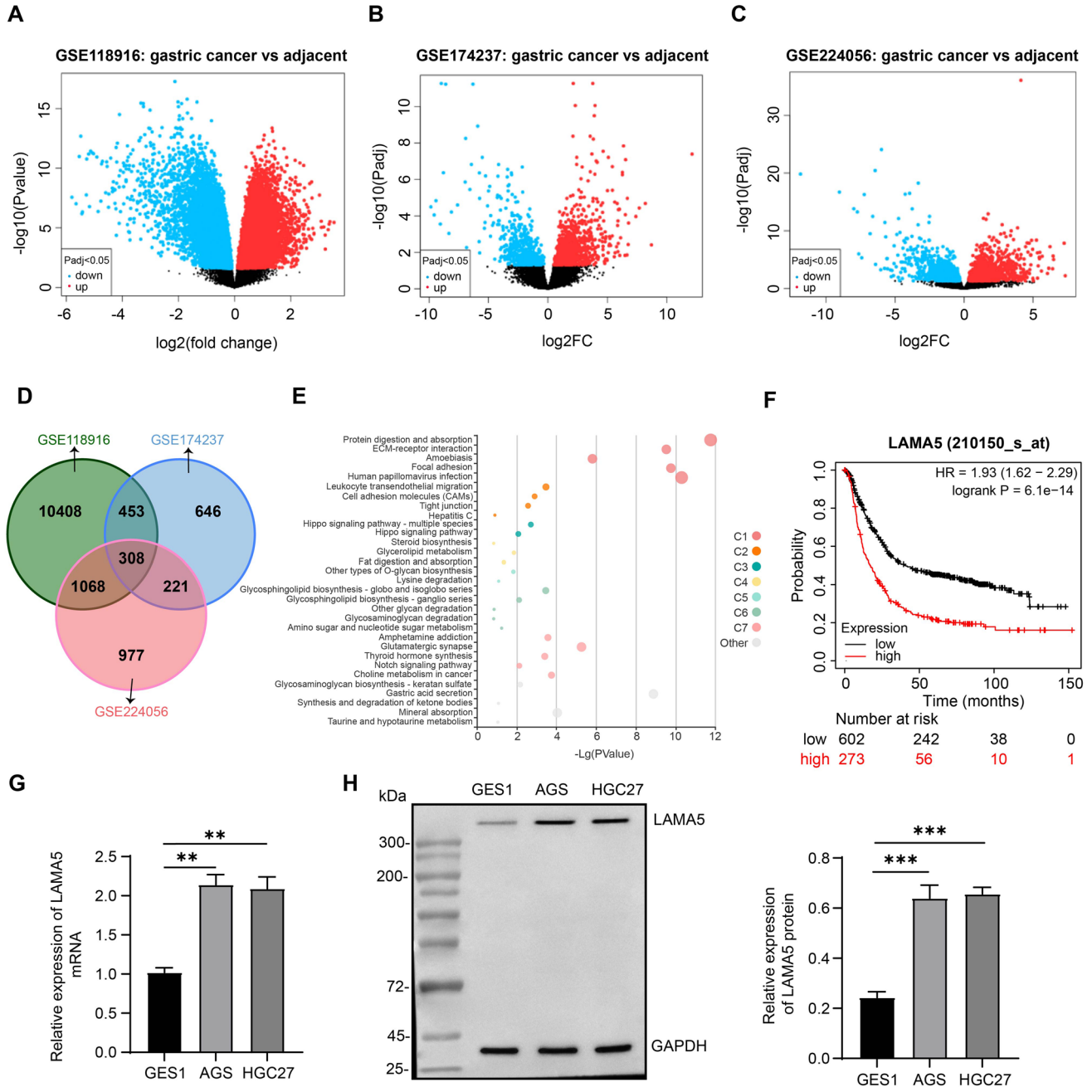

Fig. 1 LAMA5 is overexpressed in GC cell lines and predicts worse outcomes for patients in silico. **A**. The volcano map of the GSE118916 dataset. **B**. The volcano map of the GSE174237 dataset. **C**. The volcano map of the GSE224056 dataset. **D**. The intersection of differentially expressed genes in the aforementioned datasets. **E**. KEGG enrichment analysis of the 308 intersecting genes on the KOBAS website, sorted by p-value. **F**. The 5-year overall survival of GC patients with high or low LAMA5 expression was predicted on the Kaplan-Meier Plotter website. **G**. The mRNA expression of LAMA5 in GES1 and GC cells was examined using RT-qPCR. **H**. The protein expression of LAMA5 in GES1 and GC cells was examined using western blot analysis. Results are expressed as the mean ± SEM. $n = 3$ biologically independent experiments. One-way ANOVA was used for statistical analyses. $^{**}p < 0.01$, $^{***}p < 0.001$

Kaplan-Meier Plotter database (http://kmplot.com/analysis/index.php?p=background) showed that the five-year survival of patients with high expression of LAMA5 was significantly lower than that of patients with low expression (Fig. 1F).

We detected the expression of LAMA5 in GES1 cells, and human GC cells AGS and HGC27 using RT-qPCR and western blot analysis. The expression of LAMA5 was significantly higher in AGS and HGC27 cells than in GES1 cells (Fig. 1G-H).

LAMA5 promotes GC progression by activating the STAT3 signaling pathway

The LAMA5/STAT3 axis has been recently revealed to be responsible for the acinar-to-ductal cell transdifferentiation induced by cancer-associated fibroblasts in pancreatic cancer (Parte et al. 2024). Meanwhile, our previous study has identified the oncogenic role of STAT3 in GC (Cui et al. 2021). The total expression and phosphorylation of STAT3 in GES1 and GC cells AGS and HGC27 were detected by western blot analysis. Compared with GES1 cells, the expression of p-STAT3 in AGS and HGC27 was significantly increased, and there was no significant difference in total STAT3 protein expression (Fig. 2A).

To study the biological function of LAMA5 in GC cells, AGS and HGC27 cells were infected with sh-LAMA5 or sh-NC. As verified by RT-qPCR and western blot analysis, the mRNA and protein expression of LAMA5 was significantly reduced in GC cells after infection of sh-LAMA5 (Fig. 2B, C). Further western blot analysis showed that silencing of LAMA5 repressed the extent of STAT3 phosphorylation and the protein expression of Bcl-x and c-Myc in GC cells, while the pre-treatment of Colivelin rescued this decline (Fig. 2D).

Colivelin-mediated STAT3 pathway activation promotes GC progression inhibited by sh-LAMA5

The results of CCK-8, colony formation assays, and EdU assays showed that the knockdown of LAMA5 significantly reduced the OD value (Fig. 3A), colony formation (Fig. 3B), and EdU-positive cells (Fig. 3C) in GC cells, which were reversed by Colivelin treatment. The cell migration and invasion, as revealed by both wound healing assay (Fig. 3D) and Transwell assays (Fig. 3E, F), were reduced by LAMA5 downregulation and enhanced by STAT3 activation Flow cytometry showed that the percentage of apoptotic cells in the sh-LAMA5 + Colivelin group was significantly reduced compared to the sh-LAMA5 + DMSO group (Fig. 3G).

MAZ transcriptionally activates LAMA5

We predict the transcription factors of LAMA5 in the hTFtarget database (https://guolab.wchscu.cn/hTFtarget/#!/) and intersected with the differentially expressed genes in the GSE118916, GSE174237, and GSE224056 datasets. A total of four intersecting genes: NOTCH1, TEAD4, ELL2, and MAZ were obtained (Fig. 4A). A Spearman's correlation analysis of the STAD samples in the TCGA Tumor database in the GEPIA (http://gepia.cancer-pku.cn/) database showed that NOTCH1 ($R = 0.35$) and MAZ ($R = 0.28$) were significantly positively correlated with LAMA5, while TEAD4 ($R = 0.19$) and ELL2 ($R = 0.064$) were weakly associated with LAMA5 expression (Fig. 4B). Therefore, NOTCH1 and MAZ were chosen for the following study. Survival analysis by the Kaplan-Meier Plotter database revealed that the high expression of NOTCH1 ($p = 0.00024$, HR = 1.38) and MAZ ($p = 5.3 \times 10^{-9}$, HR = 1.73) both predicted the unsatisfactory prognosis of GC patients (Fig. 4C). Since the prognostic value of MAZ was more pronounced, it was chosen for the following assays. Analysis based on the JASPAR (https://jaspar.elixir.no/) database revealed binding sites on the LAMA5 promoter sequence (chr20: 62367181–62367521) that can bind to MAZ (Fig. 4D).

The expression of MAZ was highly expressed in GC cells relative to GES1 cells, as shown by RT-qPCR and western blot analysis (Fig. 4E, F). Then, AGS and HGC27 cells were infected with sh-MAZ or sh-NC, and we found that the sh-MAZ infection successfully downregulated the mRNA and protein expression of MAZ in GC cells (Fig. 4G, H).

ChIP assay showed that anti-MAZ significantly enriched the LAMA5 promoter (chr20: 62367181–62367521) in GC cells (Fig. 4I). Dual-luciferase reporter gene analysis showed that the knockdown of MAZ significantly inhibited the activity of the LAMA5 promoter in GC cells, and this effect was lost when the binding sites were mutated (Fig. 4J). RT-qPCR and western blot results showed that the mRNA level of LAMA5 was significantly reduced in the sh-MAZ group compared to the sh-NC group (Fig. 4K, L).

Knockdown of MAZ hampers GC cell growth in vivo

AGS and HGC27 cells were subjected to subcutaneous injection with stable MAZ knockdown. Tumor volumes were measured in mice every 4 days, and xenograft tumors were collected 16 days after injection. The mRNA expression of MAZ in the tumor tissues of nude mice was measured by RT-qPCR, and the mRNA level of MAZ in the tumor tissues of mice in the sh-MAZ group was significantly reduced compared with that in the sh-NC group (Fig. 5A). As a consequence, the AGS and HGC27 cells with sh-MAZ yield lighter tumors than the cells with sh-NC (Fig. 5B-D). The protein expression of Ki-67 in tumor tissues of nude mice measured by immunohistochemical staining revealed that the protein level of Ki-67 in tumor tissues of mice in the sh-MAZ group was significantly lower compared to that in the sh-NC group (Fig. 5E). In the tumor tissues, the downregulated LAMA5 mRNA (Fig. 5F) and the p-STAT3, Bcl-xl, and c-Myc protein expression (Fig. 5G) reflected that the LAMA5/STST3 axis might be the downstream target of MAZ. Finally, by TUNEL of xenograft tumors, we found that the knockdown of MAZ significantly increased the apoptosis rate of cells (Fig. 5H).

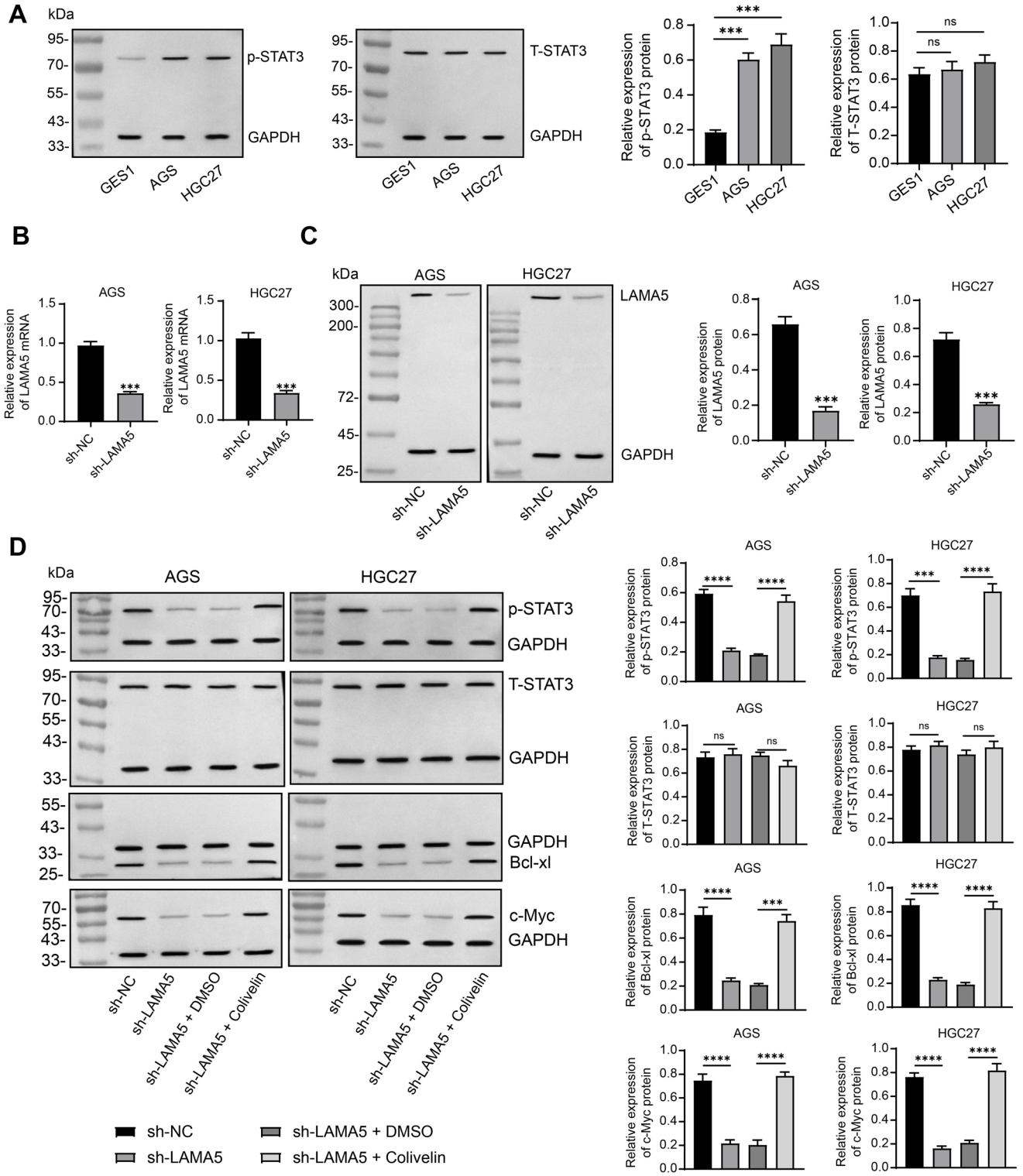

Fig. 2 LAMA5 activates the STAT3 signaling pathway in GC. **A**. The total expression and phosphorylation of STAT3 in GC cells and GSE1 cells were examined using western blot analysis. **B**. The mRNA expression of LAMA5 in GC cells infected with sh-NC or sh-LAMA5 was examined using RT-qPCR. **C**. The protein expression of LAMA5 in GC cells infected with sh-NC or sh-LAMA5 was examined using western blot analysis. **D**. The total expression and phosphorylation of STAT3, and the expression of Bcl-xl and c-Myc in GC cells infected with sh-NC, sh-LAMA5, sh-LAMA5 + DMSO, or sh-LAMA5 + Colivelin were examined using western blot analysis. Results are expressed as the mean ± SEM. $n = 3$ biologically independent experiments. Unpaired t-tests (BC) or one-way ANOVA (AD) were used for statistical analyses. ***$p < 0.001$, ****$p < 0.0001$

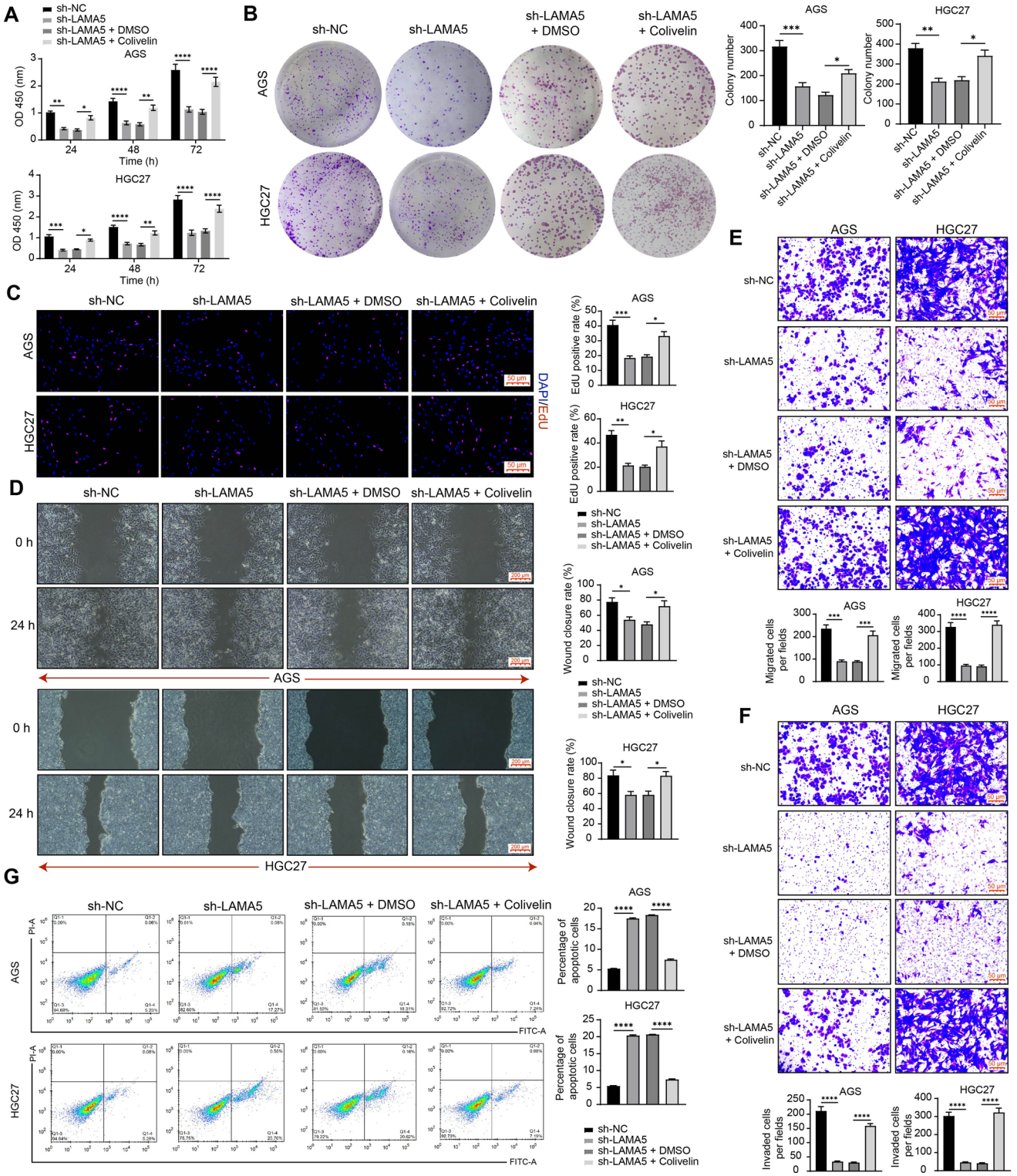

Fig. 3 The activation of STAT3 potentiates the GC cell malignant aggressiveness. **A**. Determination of GC cell viability at 24, 48, and 72 h by CCK-8 assay. **B**. The number of colonies formed was examined using colony formation assays. **C**. The viability of GC cells was examined using EdU staining. **D**. The migratory capacity of GC cells was examined using wound healing assays. The migration (**E**) and invasion (**F**) of GC cells were examined using Transwell assays. **G**. The percentage of apoptotic GC cells was examined using flow cytometry. Results are expressed as the mean ± SEM. $n = 3$ biologically independent experiments. One-way (**B-G**) or two-way ANOVA (**A**) was used for statistical analyses. *$p < 0.05$, **$p < 0.01$, ***$p < 0.001$, ****$p < 0.0001$

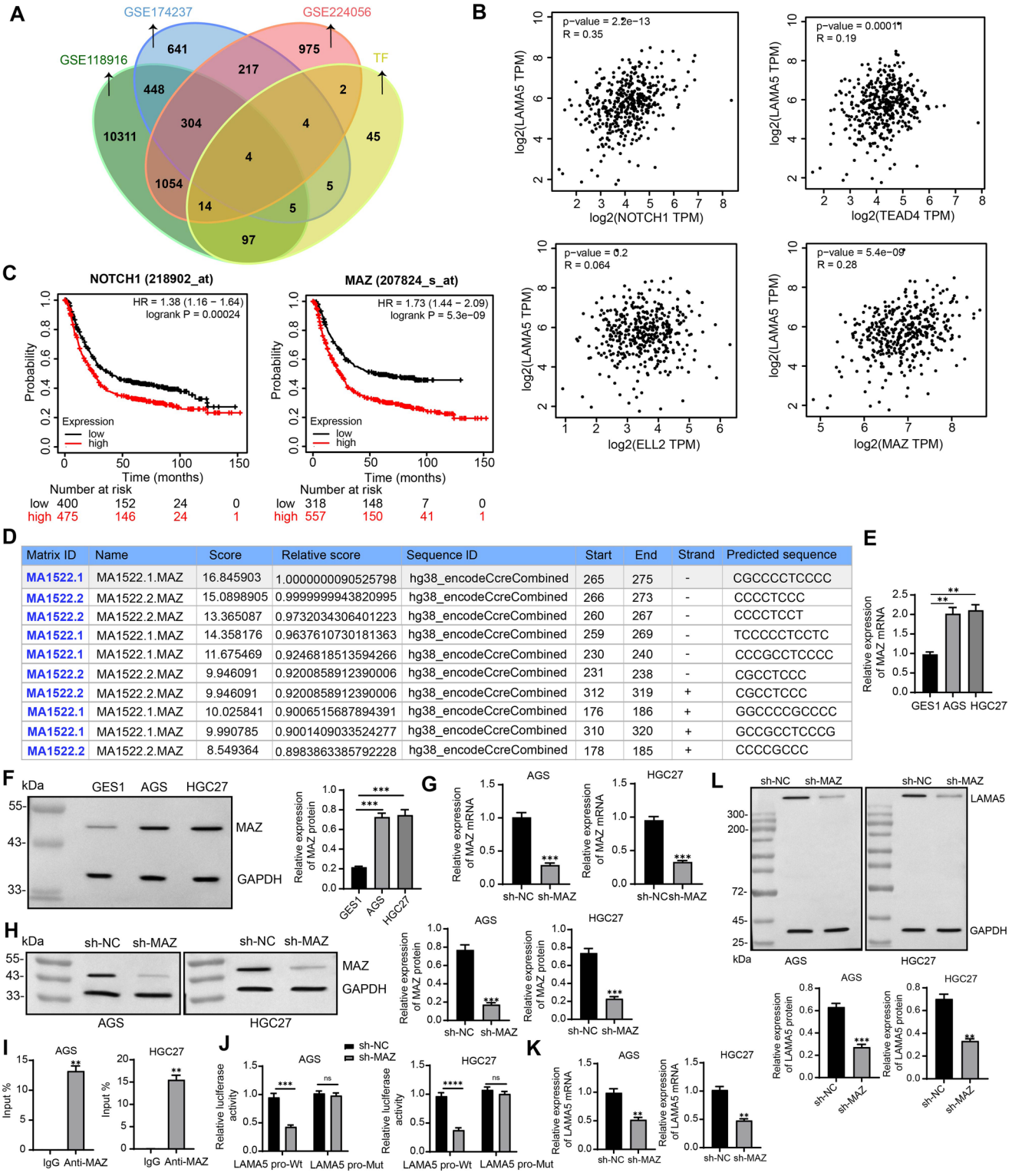

Matrix ID	Name	Score	Relative score	Sequence ID	Start	End	Strand	Predicted sequence
MA1522.1	MA1522.1.MAZ	16.845903	1.0000000090525798	hg38_encodeCcreCombined	265	275	-	CGCCCCTCCCC
MA1522.2	MA1522.2.MAZ	15.0898905	0.9999999943820995	hg38_encodeCcreCombined	266	273	-	CCCCTCCC
MA1522.2	MA1522.2.MAZ	13.365087	0.9732034306401223	hg38_encodeCcreCombined	260	267	-	CCCCTCCT
MA1522.1	MA1522.1.MAZ	14.358176	0.9637610730181363	hg38_encodeCcreCombined	259	269	-	TCCCCCTCCTC
MA1522.1	MA1522.1.MAZ	11.675469	0.9246818513594266	hg38_encodeCcreCombined	230	240	-	CCCGCCTCCCC
MA1522.2	MA1522.2.MAZ	9.946091	0.9200858912390006	hg38_encodeCcreCombined	231	238	-	CGCCTCCC
MA1522.2	MA1522.2.MAZ	9.946091	0.9200858912390006	hg38_encodeCcreCombined	312	319	+	CGCCTCCC
MA1522.1	MA1522.1.MAZ	10.025841	0.9006515687894391	hg38_encodeCcreCombined	176	186	+	GGCCCCGCCCC
MA1522.1	MA1522.1.MAZ	9.990785	0.9001409033524277	hg38_encodeCcreCombined	310	320	+	GCCGCCTCCCG
MA1522.2	MA1522.2.MAZ	8.549364	0.8983863385792228	hg38_encodeCcreCombined	178	185	+	CCCCGCCC

Fig. 4 MAZ transcriptionally activates LAMA5. **A**. The intersection of transcription factors of LAMA5 predicted in the hTFtarget database and differentially expressed genes in the GSE118916, GSE174237, and GSE224056 datasets. **B**. The Spearman's correlation analysis between LAMA5 and NOTCH1, TEAD4, ELL2, and MAZ in the STAD-TCGA database of the GEPIA database. **C**. Five-year overall survival of GC patients with high or low NOTCH1 or MAZ was predicted in the Kaplan-Meier plotter database. **D**. The binding sites between MAZ and the LAMA5 promoter were predicted in the JASPAR database. **E**. The mRNA expression of MAZ in GES1 and GC cells was examined using RT-qPCR. **F**. The protein expression of MAZ in GES1 and GC cells was examined using western blot analysis. Validation of sh-MAZ in GC cells was assessed by RT-qPCR (**G**) and western blot analysis (**H**). **I**. The enrichment of the LAMA5 promoter in the GC cells immunoprecipitated by anti-MAZ was analyzed using ChIP. **J**. Relative luciferase activity of the LAMA5 promoter (mutant or wild-type) in GC cells by dual-luciferase assay. The mRNA and protein expression of LAMA5 in GC cells infected with sh-MAZ was examined using RT-qPCR (**K**) and western blot (**L**). Results are expressed as the mean ± SEM. $n=3$ biologically independent experiments. Unpaired t-tests (**G-I**, **K-L**), one-way ANOVA (**EF**), or two-way ANOVA (**J**) were used for statistical analyses. $^{**}p<0.01$, $^{***}p<0.001$, $^{****}p<0.0001$

Overexpression of LAMA5 overturns the suppressing effects of sh-MAZ on GC cells

To further test the hypothesis that LAMA5 is a target of MAZ, we infected both AGS and HGC27 cells with sh-NC, sh-MAZ, sh-MAZ + oe-NC, or sh-MAZ + oe-LAMA5. As shown by RT-qPCR, the mRNA expression of LAMA5 was indeed restored in the presence of oe-LAMA5 (Fig. 6A). CCK-8, Colony formation assay, EdU, and Transwell assay revealed that combined overexpression of LAMA5 significantly promoted the proliferation (Fig. 6B), colony formation (Fig. 6C), viability (Fig. 6D), migration (Fig. 6E), and invasion ability in the presence of sh-MAZ (Fig. 6F) of GC cells. Apoptosis was significantly reduced in GC cells overexpressing LAMA5 (Fig. 6G). Finally, the western blot assay showed that the knockdown of MAZ significantly downregulated the expression of phosphorylated STAT3, Bcl-xl, and c-Myc, and this effect was reversed by LAMA5 overexpression (Fig. 6H).

Overexpression of LAMA5 overturns the anti-tumor effects of sh-MAZ in vivo

To reduce the number and suffering of mice, we only injected AGS cells infected with sh-MAZ + oe-NC or sh-MAZ + oe-LAMA5 into mice. The successful overexpression of LAMA5 (Fig. 7A) led to enhanced tumor volume and weight (Fig. 7B-D). The extent of STAT3 phosphorylation and the protein expression of Bcl-xl and c-Myc were increased in the presence of LAMA5 overexpression (Fig. 7E). Finally, TUNEL also showed that overexpression of LAMA5 was able to significantly reverse the pro-apoptotic effects of sh-MAZ in tumor tissues (Fig. 7F).

Discussion

Since it is often diagnosed at advanced stages with a 5-year survival rate of about 20% (Diaz Del Arco et al. 2024), a better understanding of GC pathogenesis is urgently needed. In this study, we investigated the pathological importance of LAMA5 in the progression of GC and uncovered the upstream and downstream signature molecules through which LAMA5 controls tumor aggressiveness.

Firstly, we identified LAMA5 as a differentially expressed gene in GC that both enriched to the focal adhesion pathway and has been rarely reported in GC. Consistently, Sivakumar et al. found that basal cell adhesion molecule decreased the compactness of tumor cell spheroids by inhibiting LAMA5-integrin β1 interactions in ovarian cancer (Sivakumar et al. 2023). Also enriched to the focal adhesion pathway, patients with higher LAMA4 expression had poorer overall survival than the patients with lower LAMA4 expression (Huang et al. 2023). Its counterpart LAMC1 was related to the clinical stage, tumor depth, lymph node metastasis, and distant metastasis of patients with GC, and silencing of LAMC1 repressed cell proliferation, migration, and invasion (Han et al. 2021). As for its functional role, shRNA knockdown and Cas9-mediated disruption of the LAMA5 gene dramatically reduced self-renewal and increased apoptosis of human pluripotent stem cells (Laperle et al. 2015). In this study, we further elucidated the repressed migration, invasion, viability, and apoptosis resistance in GC cells with sh-LAMA5. STAT3 has been reported to regulate its downstream target genes, including Bcl-xL and c-Myc, to promote the growth of cells, cell cycle progression, and immune suppression in addition to chemotherapy resistance (Khan et al. 2024). It was further revealed to be the downstream effector of LAMA5 in GC. Even though STAT3 has been summarized to accelerate tumor progression, metastasis, and drug resistance in gastrointestinal cancers, its upstream modifiers are generally noncoding RNAs (Ashrafizadeh et al. 2023). In this study, the activator of STAT3 was found to overturn the anti-tumor properties of sh-LAMA5, suggesting LAMA5 as a regulator of this well-known tumor-promoting pathway. Similar findings were also observed in colon cancer and anaplastic thyroid carcinoma cells where Colivelin promoted cell proliferation, migration, and invasion while inhibiting apoptosis (Gao et al. 2022; Xu et al. 2022).

Carmona-Rodríguez et al. showed that SOD3 promoted notable transcriptomic changes in tumor-stimulated endothelial cells, including the suppression of the NF-κB pathway, an inductor of LAMA5 transcription (Carmona-Rodriguez et al. 2022). Likewise, its counterpart LAMC1 has also been reported to be regulated by a transcription factor hypoxia-inducible factor-1α in glioma (Bai et al. 2024). In the study here, MAZ was determined as a transcription

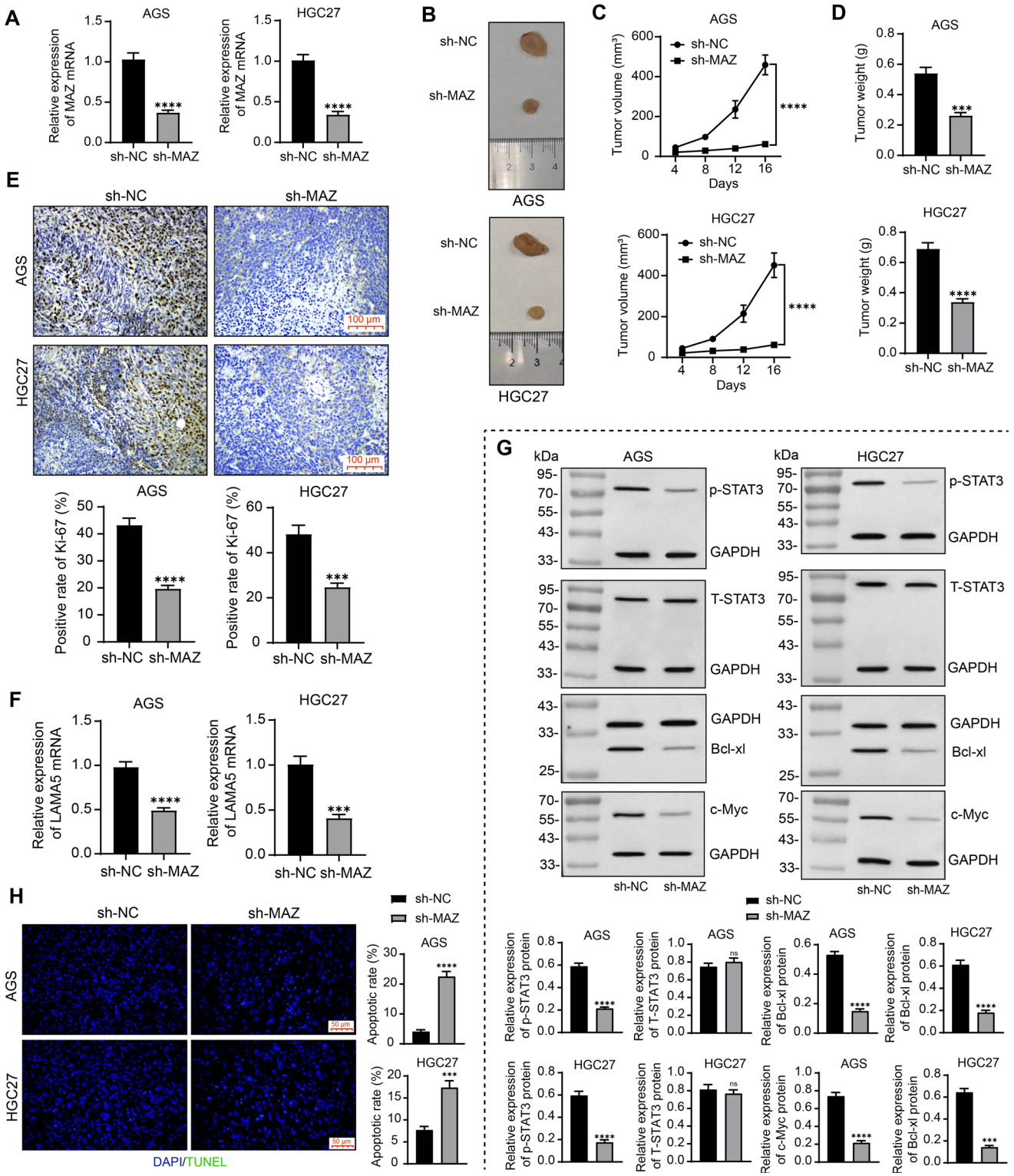

Fig. 5 Knockdown of MAZ disturbs the tumor growth in vivo. **A**. The mRNA expression of MAZ in tumor tissues derived from GC cells infected with sh-NC or sh-MAZ was examined using RT-qPCR. **B**. The representative images of tumors harvested from mice. **C**. The tumor growth curve during the 16-d period. **D**. Mouse xenograft tumor weights measured at day 16. **E**. Positive rate of Ki-67 in the tumor tissues harvested from mice. **F**. The mRNA expression of LAMA5 in tumor tissues derived from GC cells infected with sh-NC or sh-MAZ was examined using RT-qPCR. **G**. The total expression and phosphorylation of STAT3 and the expression of Bcl-xl and c-Myc in tumor tissues derived from GC cells infected with sh-NC or sh-MAZ were examined using western blot analysis. **H**. Apoptosis in xenograft tumors was assessed using TUNEL. Results are expressed as the mean ± SEM. $n = 5$ biologically independent experiments. Unpaired t-tests (**A**, **D**-**H**) or two-way ANOVA (**C**) were used for statistical analyses. ***$p < 0.001$, ****$p < 0.0001$

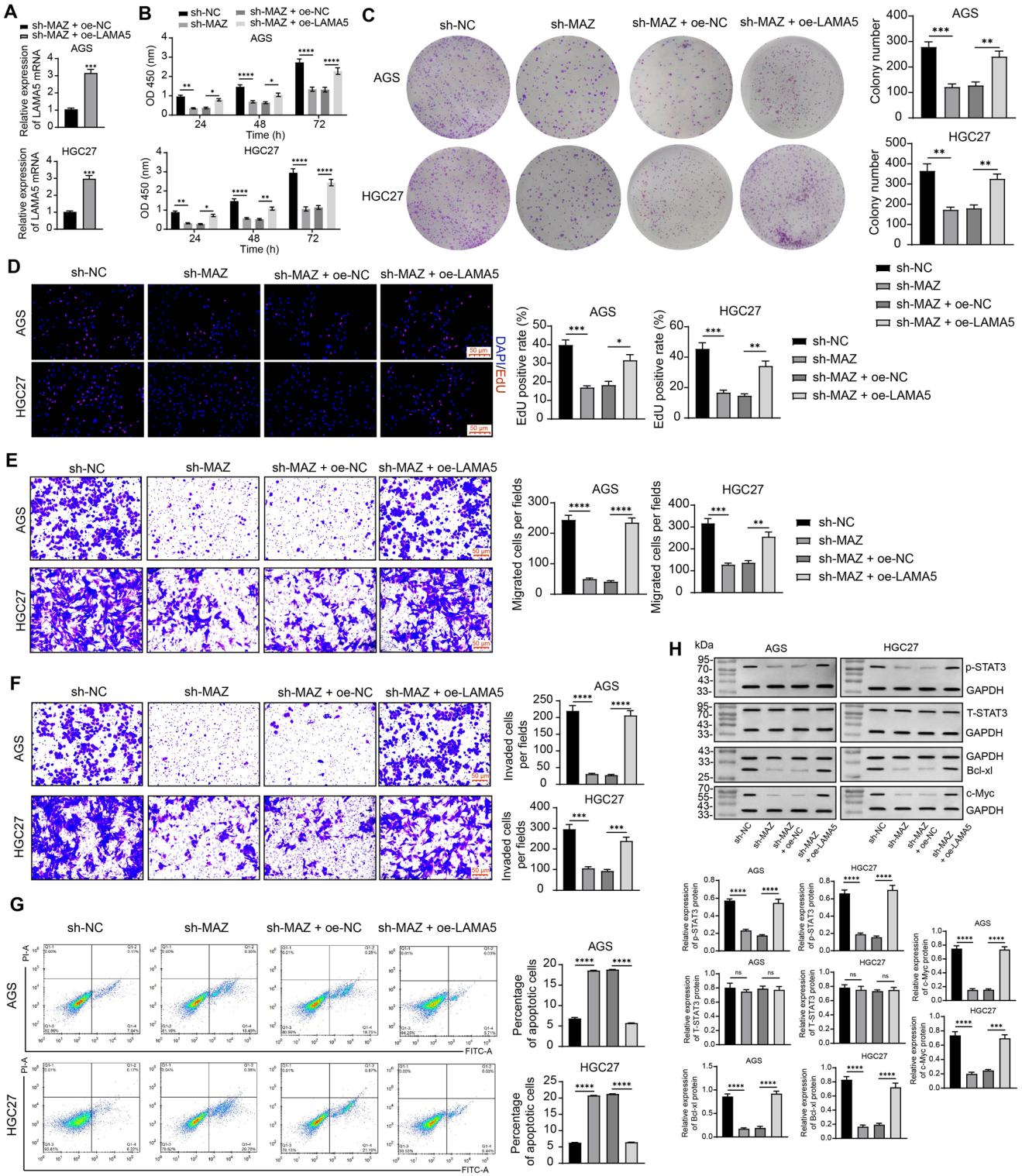

Fig. 6 Overexpression of LAMA5 overturns the inhibitory effects of sh-MAZ on GC cells in vitro. **A**. The mRNA expression of LAMA5 in GC cells infected with sh-MAZ + oe-NC or oe-LAMA5 was examined using RT-qPCR. **B**. Determination of GC cell viability at 24, 48, and 72 h by CCK-8 assay. **C**. The number of colonies formed was examined using colony formation assays. **D**. The viability of GC cells was examined using EdU staining. The migration (**E**) and invasion (**F**) of GC cells were examined using Transwell assays. **G**. The percentage of apoptotic GC cells was examined using flow cytometry. **H**. The total expression and phosphorylation of STAT3 and the expression of Bcl-xl and c-Myc in GC cells were examined using western blot analysis. Results are expressed as the mean ± SEM. $n = 3$ biologically independent experiments. Unpaired t-tests (**A**) and one-way (**C**-**H**) or two-way ANOVA (**B**) were used for statistical analyses. *$p < 0.05$, **$p < 0.01$, ***$p < 0.001$, ****$p < 0.0001$

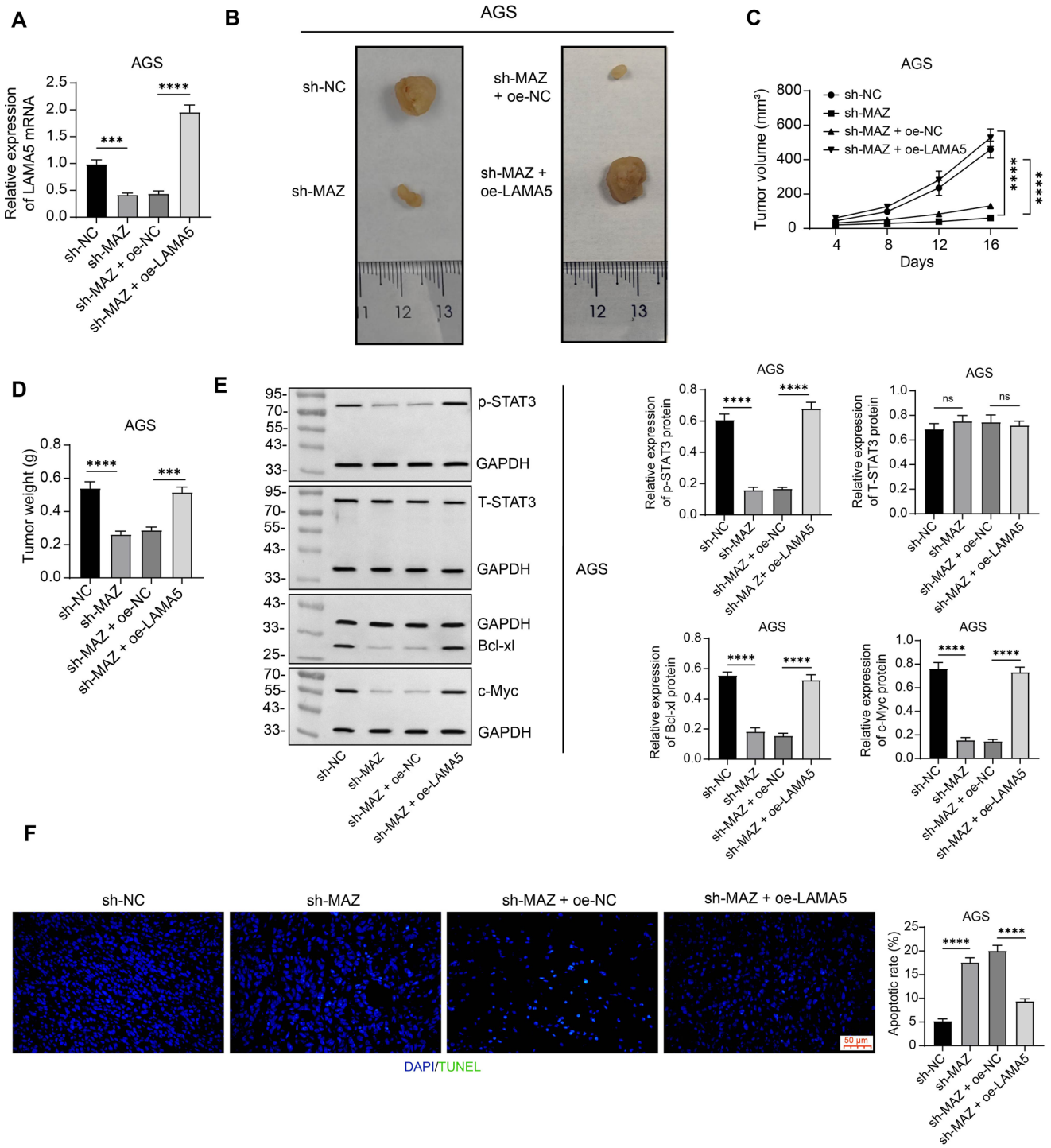

Fig. 7 Overexpression of LAMA5 overturns the anti-tumor effects of sh-MAZ. **A**. The mRNA expression of LAMA5 in tumor tissues derived from GC cells infected with sh-MAZ + oe-NC or oe-LAMA5 was examined using RT-qPCR. **B**. The representative images of tumors harvested from mice. **C**. The tumor growth curve during the 16-d period. **D**. Mouse xenograft tumor weights measured at day 16. **E**. The total expression and phosphorylation of STAT3 and the expression of Bcl-xl and c-Myc in tumor tissues derived from GC cells infected with sh-MAZ + oe-NC or oe-LAMA5 were examined using western blot analysis. **F**. Apoptosis in xenograft tumors was assessed using TUNEL. Results are expressed as the mean ± SEM. $n = 5$ biologically independent experiments. One way (**A**, **D**-**F**) or two-way ANOVA (**C**) were used for statistical analyses. ***$p < 0.001$, ****$p < 0.0001$

factor that is responsible for the overexpression of LAMA5 in GC. Dysregulated transcription factors accentuated activated transcriptional regulation in non-alcoholic fatty liver disease-associated liver cancer, particularly the enrichment of MAZ-MYC activities (Wong et al. 2022), Moreover, G-quadruplexes recruited MAZ to the CCND1 promoter to upregulate CCND1 expression and aggravated hepatocarcinogenesis (Wang et al. 2024). Guetta-Terrier et al. showed that suppression of MAZ downregulated genes with high expression that exhibit significant cell state transitions after treatment with Chi3l1, and MAZ deficiency rescued the Chi3L-induced increase of glioma stem cell self-renewal (Guetta-Terrier et al. 2023). These findings highlighted the role of MAZ as a transcription factor in different cancers. In addition, Maity et al. found that MAZ depletion in pancreatic cancer cells inhibited the epithelial-to-mesenchymal transition, migration, invasion, and sphere-forming ability of pancreatic cancer cells (Maity et al. 2018). More relevantly, the expression of MAZ was high in GC cells compared with normal human gastric mucosal epithelial cells, and downregulation of MAZ inhibited the proliferation and migration of GC cells and induced apoptosis (Zhao et al. 2021). Interestingly, MAZ expression supported tumorigenesis in inflammation-induced colon cancer and was of great importance for the growth of human colon cancer cells by regulating oncogenic STAT3 signaling (Triner et al. 2018). Here, we substantiated the bind relation between MAZ and the LAMA5 promoter and also observed the impaired STAT3 signaling in the presence of sh-MAZ in GC cells. Furthermore, the anti-tumor effects of sh-MAZ in vitro and in vivo were both found to be reversed by the overexpression of LAMA5, further supporting that MAZ plays an oncogenic role in GC by inducing the expression of LAMA5 and the activation of the STAT3 signaling.

Notably, the protein digestion and absorption pathway has the highest p-value enriched by the differentially expressed genes in the three GEO datasets included in this study. This pathway has a profound influence on gut microbiota and food processing (Loveday 2023), thereby impacting gastrointestinal cancer. Therefore, differentially expressed genes enriched in this pathway need to be further explored.

This study demonstrates the biological function of LAMA5 in GC. Our investigation revealed that the knockdown of LAMA5 repressed the malignant phenotype of GC cells and slowed the tumor growth. More importantly, we confirmed the existence of a MAZ/LAMA5/STAT3 axis in the GC progression. Therefore, therapeutic strategies based on inhibition of this axis may be a promising approach for GC treatment.

Acknowledgements We thank the Youthful Science Foundation of Shandong Province of China (BS2013YY045); and the China Postdoctoral Science Foundation (2014M560561) for funding support.

Author contributions YW designed and performed the research. JZX analyzed the data and wrote the paper. HXZ analyzed the data. XBG analyzed the data and edited the manuscript. HJL and QHS designed the research, analyzed the data, and wrote the paper.

Funding This work was supported by the Youthful Science Foundation of Shandong Province of China (BS2013YY045); and the China Postdoctoral Science Foundation (2014M560561).

Data availability The data used to support the findings of this study are available from the corresponding author upon request.

Declarations

Ethics approval Animal experiments were approved by the Animal Care and Ethics Committee of Shandong Provincial Hospital Affiliated to Shandong First Medical University (approval no. KT2024-01-15-01) and conducted following the NIH Guide for the Care and Use of Laboratory Animals.

Consent for publication Not applicable.

Competing interests The authors declare no competing interests.

References

Alsina M, Arrazubi V, Diez M, Tabernero J (2023) Current developments in gastric cancer: from molecular profiling to treatment strategy. Nat Rev Gastroenterol Hepatol 20:155–170. https://doi.org/10.1038/s41575-022-00703-w

Ashrafizadeh M et al (2023) Noncoding RNAs as regulators of STAT3 pathway in Gastrointestinal cancers: roles in cancer progression and therapeutic response. Med Res Rev 43:1263–1321. https://doi.org/10.1002/med.21950

Bai J et al (2024) HIF-1alpha-mediated LAMC1 overexpression is an unfavorable predictor of prognosis for glioma patients: evidence from pan-cancer analysis and validation experiments. J Transl Med 22:391. https://doi.org/10.1186/s12967-024-05218-3

Carmona-Rodriguez L, Martinez-Rey D, Martin-Gonzalez P, Franch M, Sorokin L, Mira E, Manes S (2022) Superoxide Dismutase-3 downregulates laminin alpha5 expression in tumor endothelial cells via the Inhibition of nuclear factor kappa B signaling cancers (Basel). 14. https://doi.org/10.3390/cancers14051226

Cheng L et al (2024) LAMC2 regulates the proliferation, invasion, and metastasis of gastric cancer via PI3K/Akt signaling pathway. J

Cancer Res Clin Oncol 150:230. https://doi.org/10.1007/s00432-024-05720-7
Chiu WC et al (2016) The synthetic beta-Nitrostyrene derivative CYT-Rx20 inhibits esophageal tumor growth and metastasis via PI3K/AKT and STAT3 pathways. PLoS ONE 11:e0166453. https://doi.org/10.1371/journal.pone.0166453
Christodoulidis G, Koumarelas KE, Kouliou MN, Thodou E, Samara M (2024) Gastric Cancer in the era of epigenetics. Int J Mol Sci 25. https://doi.org/10.3390/ijms25063381
Cui N et al (2021) Long non-coding RNA LINC00511 regulates the expression of microRNA-625-5p and activates signal transducers and activators of transcription 3 (STAT3) to accelerate the progression of. Gastric cancer Bioengineered 12:2915–2927. https://doi.org/10.1080/21655979.2021.1940611
Diao B, Sun C, Yu P, Zhao Z, Yang P (2023) LAMA5 promotes cell proliferation and migration in ovarian cancer by activating Notch signaling pathway. FASEB J 37:e23109. https://doi.org/10.1096/fj.202300306R
Diaz Del Arco C, Fernandez Acenero MJ, Ortega Medina L (2024) Molecular classifications in gastric cancer: A call for interdisciplinary collaboration. Int J Mol Sci 25. https://doi.org/10.3390/ijms25052649
Eke I, Cordes N (2015) Focal adhesion signaling and therapy resistance in cancer. Semin Cancer Biol 31:65–75. https://doi.org/10.1016/j.semcancer.2014.07.009
Gao H, Wang W, Li Q (2022) GANT61 suppresses cell survival, invasion and epithelial-mesenchymal transition through inactivating AKT/mTOR and JAK/STAT3 pathways in anaplastic thyroid carcinoma. Cancer Biol Ther 23:369–377. https://doi.org/10.1080/15384047.2022.2051158
Guan WL, He Y, Xu RH (2023) Gastric cancer treatment: recent progress and future perspectives. J Hematol Oncol 16:57. https://doi.org/10.1186/s13045-023-01451-3
Guetta-Terrier C et al (2023) Chi3l1 is a modulator of glioma stem cell States and a therapeutic target in. Glioblastoma Cancer Res 83:1984–1999. https://doi.org/10.1158/0008-5472.CAN-21-3629
Han ZR, Jiang XL, Fan WC (2021) LAMC1 is related to the poor prognosis of patients with gastric cancer and facilitates cancer. Cell Malignancies Neoplasma 68:711–718. https://doi.org/10.4149/neo_2021_201117N1239
Huang FY et al (2023) FAT4 loss initiates hepatocarcinogenesis through the switching of canonical to noncanonical WNT signaling pathways hepatol commun. 7. https://doi.org/10.1097/HC9.0000000000000338
Khan F, Pandey P, Verma M, Upadhyay TK (2024) Terpenoid-Mediated targeting of STAT3 signaling in cancer: an overview of preclinical studies biomolecules. 14. https://doi.org/10.3390/biom14020200
Laperle A, Hsiao C, Lampe M, Mortier J, Saha K, Palecek SP, Masters KS (2015) alpha-5 laminin synthesized by human pluripotent stem cells promotes Self-Renewal. Stem Cell Rep 5:195–206. https://doi.org/10.1016/j.stemcr.2015.06.009
Li M et al (2022) Establishment and analysis of an individualized Immune-Related gene signature for the prognosis of gastric. Cancer Front Surg 9:829237. https://doi.org/10.3389/fsurg.2022.829237
Loveday SM (2023) Protein digestion and absorption: the influence of food processing. Nutr Res Rev 36:544–559. https://doi.org/10.1017/S0954422422000245
Lu Y, Kong X, Zhong W, Hu M, Li C (2021) Diagnostic, therapeutic, and prognostic value of the thrombospondin family in gastric Cancer. Front Mol Biosci 8:647095. https://doi.org/10.3389/fmolb.2021.647095
Maity G et al (2018) The MAZ transcription factor is a downstream target of the oncoprotein Cyr61/CCN1 and promotes pancreatic cancer cell invasion via CRAF-ERK signaling. J Biol Chem 293:4334–4349. https://doi.org/10.1074/jbc.RA117.000333
Parte S et al (2024) Cancer-Associated Fibroblast Induces Acinar-to-Ductal Cell Transdifferentiation and Pancreatic Cancer Initiation Via LAMA5/ITGA4 Axis Gastroenterology 166:842–858 e845 https://doi.org/10.1053/j.gastro.2023.12.018
Romer AMA, Thorseth ML, Madsen DH (2021) Immune modulatory properties of collagen in. Cancer Front Immunol 12:791453. https://doi.org/10.3389/fimmu.2021.791453
Sivakumar S et al (2023) Basal cell adhesion molecule promotes metastasis-associated processes in ovarian cancer. Clin Transl Med 13:e1176. https://doi.org/10.1002/ctm2.1176
Sun B, Ding B, Chen Y, Peng C, Chen X (2023) AFAP1L1 promotes gastric cancer progression by interacting with VAV2 to facilitate CDC42-mediated activation of ITGA5 signaling pathway. J Transl Med 21:18. https://doi.org/10.1186/s12967-023-03871-8
Tahara E (1990) Growth factors and oncogenes in human Gastrointestinal carcinomas. J Cancer Res Clin Oncol 116:121–131. https://doi.org/10.1007/BF01612665
Thrift AP, Wenker TN, El-Serag HB (2023) Global burden of gastric cancer: epidemiological trends, risk factors, screening and prevention Nat. Rev Clin Oncol 20:338–349. https://doi.org/10.1038/s41571-023-00747-0
Triner D et al (2018) Myc-Associated zinc finger protein regulates the Proinflammatory response in colitis and Colon cancer via STAT3 signaling. Mol Cell Biol 38. https://doi.org/10.1128/MCB.00386-18
Wang W et al (2024) G-quadruplexes promote the motility in MAZ phase-separated condensates to activate CCND1 expression and contribute to hepatocarcinogenesis. Nat Commun 15:1045. https://doi.org/10.1038/s41467-024-45353-5
Wong AM et al (2022) Unique molecular characteristics of NAFLD-associated liver cancer accentuate beta-catenin/TNFRSF19-mediated immune evasion. J Hepatol 77:410–423. https://doi.org/10.1016/j.jhep.2022.03.015
Xu T et al (2022) LINC00858 promotes colon cancer progression through activation of STAT3/5 signaling by recruiting transcription factor RAD21 to upregulate. PCNP Cell Death Discov 8:228. https://doi.org/10.1038/s41420-022-00832-w
Yang Q et al (2019) MAZ promotes prostate cancer bone metastasis through transcriptionally activating the KRas-dependent RalGEFs. Pathw J Exp Clin Cancer Res 38:391. https://doi.org/10.1186/s13046-019-1374-x
Yao Y (2017) Laminin: loss-of-function studies. Cell Mol Life Sci 74:1095–1115. https://doi.org/10.1007/s00018-016-2381-0
Yu ZH et al (2017) Dual function of MAZ mediated by FOXF2 in basal-like breast cancer: promotion of proliferation and suppression of progression. Cancer Lett 402:142–152. https://doi.org/10.1016/j.canlet.2017.05.020
Zhao X, Ye N, Feng X, Ju H, Liu R, Lu W (2021) MicroRNA-29b-3p inhibits the migration and invasion of gastric Cancer cells by regulating the Autophagy-Associated protein. MAZ Onco Targets Ther 14:3239–3249. https://doi.org/10.2147/OTT.S274215
Zheng C et al (2023) Myc-Associated zinc finger protein promotes metastasis of papillary thyroid Cancer front biosci. (Landmark Ed) 28:162. https://doi.org/10.31083/j.fbl2808162